

Oxygen adsorption at $\text{La}_{1-x}\text{Sr}_x\text{MnO}_3(001)$ surfaces: Predictions from first principles

Sergei Piskunov,^{1,2,3,*} Timo Jacob,⁴ and Eckhard Spohr⁵¹*Faculty of Computing, University of Latvia, 19 Raina Blvd., Riga LV-1586, Latvia*²*Faculty of Physics and Mathematics, University of Latvia, 8 Zellu Street, Riga LV-1002, Latvia*³*Institute for Solid State Physics, University of Latvia, 8 Kengaraga Street, Riga LV-1063, Latvia*⁴*Institute of Electrochemistry, Ulm University, D-89069 Ulm, Germany*⁵*Department of Theoretical Chemistry, University of Duisburg-Essen, Universitatstr. 2, D-45141 Essen, Germany*

(Received 21 November 2010; published 9 February 2011)

The interaction of atomic and molecular oxygen with MnO_2 - and $\text{La}(\text{Sr})\text{O}$ -terminated (001) surfaces of Sr-doped LaMnO_3 has been studied using the B3LYP hybrid exchange–correlation functional within the framework of density functional theory (DFT). Using the obtained binding energies in conjunction with the *ab initio* thermodynamics we predict that adsorbed O atoms stabilize the surface of an LSM cathode at typical SOFC working conditions ($T = 1100$ K, $p_{\text{O}_2} = 0.2 p_0$). The most favorable oxygen adsorption sites have been found to be atop surface Mn atoms on the MnO_2 -terminated surface and on the hollow positions of the $\text{La}(\text{Sr})\text{O}$ -terminated LSM(001) surface. An O_2 molecule adsorbed at a hollow position of the $\text{La}(\text{Sr})\text{O}$ -terminated surface is readily dissociated, which adds a substantial contribution to the ionic transport at the LSM surface.

DOI: [10.1103/PhysRevB.83.073402](https://doi.org/10.1103/PhysRevB.83.073402)

PACS number(s): 71.15.Mb, 73.20.Hb

Because of excellent electrocatalytic activity for the oxygen reduction reaction (ORR) at high temperatures, good electronic conductivity, and chemical stability at operation conditions, Sr-doped LaMnO_3 ($\text{La}_{1-x}\text{Sr}_x\text{MnO}_3$, $0.1 \leq x \leq 0.2$; hereafter denoted as LSM) is one of the most popular materials for cathodes in solid oxide fuel cells (SOFCs).^{1,2} For the best performance in state-of-the-art applications, LSM is mixed with ionic conductors (such as, e.g., yttria-stabilized zirconia) to form composite cathodes.³ Alternatively, dense thin film LSM electrodes are proposed for micro-SOFCs operating at temperatures below 1000 K.⁴ The development of highly efficient SOFCs relies on the fundamental understanding of the ORR process at the electrode/electrolyte interface. The cathodic reaction comprises first the (dissociative) adsorption of an oxygen molecule on the LSM surface, followed by surface or bulk diffusion toward the electrolyte and ion incorporation into the electrolyte. In spite of the fact that atomistic simulations are providing new insights into understanding transport processes at the surfaces of complex oxides, results obtained from *ab initio* modeling on LSM cathodes under real operating conditions are scarce in the literature. Very recently, based on results of DFT simulations on oxygen adsorption and defect migration on LaMnO_3 (001) surfaces,^{5,6} several of the most probable ORR pathways for MnO_2 -terminated LSM cathodes were suggested. Transition states for the ORR have been predicted from first principle for the (001) and (110) surfaces of LSM ($x = 0.5$),^{7–9} as well as for some other perovskites of the $\text{La}_{0.5}\text{Sr}_{0.5}\text{BO}_3$ group.¹⁰

In the present paper we report large-scale first principles calculations of atomic and molecular oxygen adsorbed on the most stable $\text{La}(\text{Sr})\text{O}$ - and MnO_2 -terminated LSM (001) surfaces¹¹ [henceforth denoted as $\text{La}\text{-LSM}(001)$ and $\text{Mn}\text{-LSM}(001)$, respectively] with the Sr concentrations ($x = 0.125$ and $x = 0.1$) chosen to be relevant for realistic SOFC cathodes. In order to avoid considerable errors caused by neglecting spin polarization in manganites,^{5,12} LSM surfaces of both terminations have been calculated in A-type anti-ferromagnetic (A-AFM) ground states, i.e., Mn spins are

parallel within the basal plane and antiparallel in neighboring planes.^{11,13} For the present *ab initio* calculations we used DFT-HF hybrid exchange–correlation functionals, which were shown to yield reliable results for the electronic and atomic structure both for bulk LSM¹³ and its (001) surfaces.¹¹ We employ the hybrid B3LYP exchange–correlation functional.¹⁴ The calculations were carried out with the CRYSTAL computer code,¹⁵ with atom-centered Gaussian-type functions as basis set (BS). The computational details are thoroughly discussed in Refs. 11,13. For La we have employed an extended BS with additional *f*-type orbitals. Reciprocal space integration was performed by sampling the Brillouin zone with the 4×4 Pack–Monkhorst mesh.¹⁶ All atoms in the slab unit cells (including adsorbate atoms) were allowed to relax. Oxygen adsorbates placed above the selected surface structures (see Fig. 1) correspond to a coverage of 12.5%. All calculations have been performed spin-polarized. The effective charges on atoms as well as net bond populations have been calculated according to the Mulliken population analysis.¹⁵

We adopted the atomistic thermodynamics approach to predict oxygen adsorption on LSM surfaces at temperatures relevant to SOFC operation. The thermodynamic stability diagrams for the clean and adsorbate covered LSM(001) surfaces were calculated by the methodology thoroughly discussed in Ref. 11. The Gibbs free energy of formation of the relevant oxygen species on the LSM(001) surface can be defined as⁶

$$\Delta G^{\text{ads}}(T, p_{\text{O}_2}) \approx \Delta E^{\text{ads}} - \Delta \mu_{\text{O}}(T, p_{\text{O}_2}), \quad (1)$$

where

$$\Delta E^{\text{ads}} = \frac{1}{2}(E_{\text{slab}}^{\text{ads}} - 2E^{\text{ads}} - E_{\text{slab}}) \quad (2)$$

is the oxygen adsorption energy calculated by DFT as the energy difference between the adsorbate covered slab $E_{\text{slab}}^{\text{ads}}$ and the sum of the energies of the clean slab E_{slab} and the energy of an oxygen atom in the free oxygen molecule (i.e., $E^{\text{ads}} = \frac{1}{2}E_{\text{O}_2}$ for atomic oxygen adsorption and $E^{\text{ads}} = E_{\text{O}_2}$ for molecular

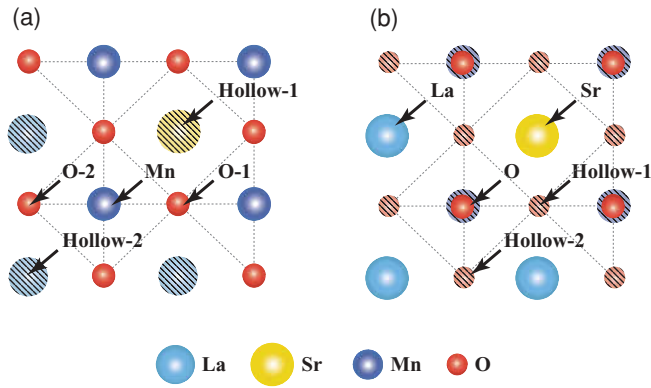


FIG. 1. (Color online) Schematic representation of oxygen adsorption sites examined in the present study: Top view of (a) the MnO_2 -terminated LSM(001) surface and of (b) the La(Sr)-O-terminated LSM(001) surface. Hatched circles denote atoms in the subsurface plane. Surfaces under consideration are discussed in details in Ref. 11.

oxygen adsorption). The factor $\frac{1}{2}$ enters Eq. (2) because each of our slabs contains two equivalent surfaces. Note that entropy contributions are dominated by the surrounding O_2 gas, that is why it is justified to use adsorption energies instead of adsorption free energies. Negative values of ΔE^{ads} correspond to energetically favorable adsorption.

$\Delta\mu_{\text{O}}(T, p_{\text{O}_2})$ is the variation of oxygen chemical potential due to temperature and pressure of the surrounding oxygen atmosphere. In addition to the experimental variation it contains a correction term $\delta\mu_{\text{O}}^0 = 0.4$ eV, which compensates the difference between the experimentally determined variation of the oxygen chemical potential and the reference state in current theoretical calculations (see Refs. 17 and 6 for a thorough discussion). The Gibbs free energies vary with T and p_{O_2} only due to the dependence of the oxygen chemical potential on these parameters in the gas phase. From experiment we know that the rate of oxygen exchange for LSM cathodes is insensitive to changes in p_{O_2} and strongly dependent on temperature.¹⁸ Thus $\Delta\mu_{\text{O}}(T, p_{\text{O}_2})$ can be related to the SOFC operating temperatures at the ambient O_2 partial pressure $p_{\text{O}_2} = 0.2p_0$ (with $p_0 = 1$ atm). This yields values of $\Delta\mu_{\text{O}}$ of -1.43 , -1.57 , -1.71 , and -1.84 eV at temperatures of 900, 1000, 1100, and 1200 K, respectively.

Figure 1 shows a schematic top view of possible oxygen adsorption sites on the Mn-LSM(001) slab with Sr dopant at $x = 0.125$ in the subsurface plane (a) and on the La-LSM(001) slab with Sr dopant at $x = 0.1$ in the surface plane (b). We found these surface structures to be the thermodynamically most stable ones at room temperature and normal pressure, while at a typical SOFC operating temperature of 1100 K only La-LSM(001) is predicted to be stable.¹¹ Mn-LSM(001) has also been taken into consideration here, because it is attractive for the oxygen incorporation process due to smaller oxygen vacancy formation energy. [The Gibbs free energies of vacancy formation $\Delta G^{\text{vac}}(1100\text{ K}, 0.2p_0)$ have been estimated to be 0.76 eV for the MnO_2 -terminated vs 2.35 eV for the La(Sr)O-terminated surface, and 1.45 eV for LSM bulk at $x = 0.125$.] In Fig. 1 the O-1 and O-2, as well as the Hollow-1 and Hollow-2 adsorption sites differ by their proximity to the Sr dopant.

The thermodynamic stability diagram plotted in Fig. 2(a) shows the regions of stability of clean and oxygen covered LSM(001) surfaces with respect to precipitation of oxides and perovskites from LSM. The phase diagram indicates that at SOFC operating conditions (1100 K, $p = 0.2p_0$) atomic oxygen adsorbed at the Hollow-2 position of La-LSM(001) possesses the lowest free energy of all studied surfaces, and thus leads to a stabilization of La-LSM(001).

Figure 2(b) shows the thermodynamic stability diagram along the line corresponding to precipitation of SrO oxide as a function of $\Delta\mu_{\text{Mn}}$ and temperature. Here $\Delta\mu_{\text{La}}$ was eliminated via

$$\Delta\mu_{\text{La}} = \frac{1}{1-x_b} E_{\text{LSM}}^f - \frac{x_b}{1-x_b} E_{\text{SrO}}^f, \quad (3)$$

where $x_b = 0.125$ is the Sr concentration in LSM bulk, E_{LSM}^f and E_{SrO}^f are the formation energies of LSM and SrO, respectively (see Ref. 11 for more details). The variation of oxygen chemical potential has been translated into a function of partial O_2 pressure and temperature using thermodynamical tables¹⁹ (see Refs. 6,20 for detailed prescription). In agreement with Ref. 6 we observe that Mn-LSM(001) can be stabilized by atomic oxygen adsorbate, but only at relatively low temperatures of ~ 50 K. In the same temperature range the La-LSM(001) is stabilized by chemisorbed O_2 molecules. In the temperature range between ~ 50 K and ~ 1150 K oxygen atoms chemisorbed at the Hollow-2 position of the La-LSM(001) stabilize the La(Sr)O termination. At even higher temperatures the bare La-LSM(001) is stable in agreement with our predictions in Ref. 11.

Table I lists the calculated adsorption properties of O atoms on LSM(001) surfaces. In agreement with Refs. 5 and 21, Mn-LSM(001) exhibits a strong preference for O-atom adsorption atop of surface Mn atoms. Surface Mn and surrounded surface oxygens donate 0.56e to the adsorbate, thereby forming an O^I chemisorbed species (the calculated Mulliken charge for the formal O^{-II} in LSM bulk is $-1.42e$). The increased $\text{Mn}^{\text{surf}} - \text{O}^{\text{ads}}$ bond population (0.30 vs. 0.08 e for LSM bulk) and relatively short $\text{Mn}^{\text{surf}} - \text{O}^{\text{ads}}$ bond lengths (1.58 vs 1.92 Å for LSM bulk) indicate a strongly covalent nature of the bond between adsorbate and surface ion. Atomic oxygen adsorbed on O-1 and O-2 adsorption sites leads to a weakly bonded O_2^I surface molecule (negative bond populations indicate antibonding contributions). The difference in the charge transferred from O-1 and O-2 adsorption sites to O^{ads} is caused by the vicinity of the polarizing Sr^{2+} dopant and the large relaxation of the surface upon O adsorption. Note that chemisorption of atomic O on Mn-LSM(001) is endothermic at SOFC operating temperatures. Atomic O adsorption at these conditions is exothermic only for the hollow positions of La-LSM(001), where a slight preference for the Hollow-2 site is observed. La-LSM(001) is hypostoichiometric in oxygen; it thus readily reduces O adsorbates formally to the O^{-II} stage.

We also studied the adsorption of O_2 molecules on the most energetically favorable adsorption sites at both surface terminations (Table I). O_2 chemisorption on La-LSM(001) surfaces is less endothermic than on MnO_2 -terminated surfaces; it clearly indicates the formation of $\text{O}_2^I - \text{O}_2^{-II}$ like surface species with an elongated bond length and antibonding nature. This surface molecule is easily dissociated, thus contributing

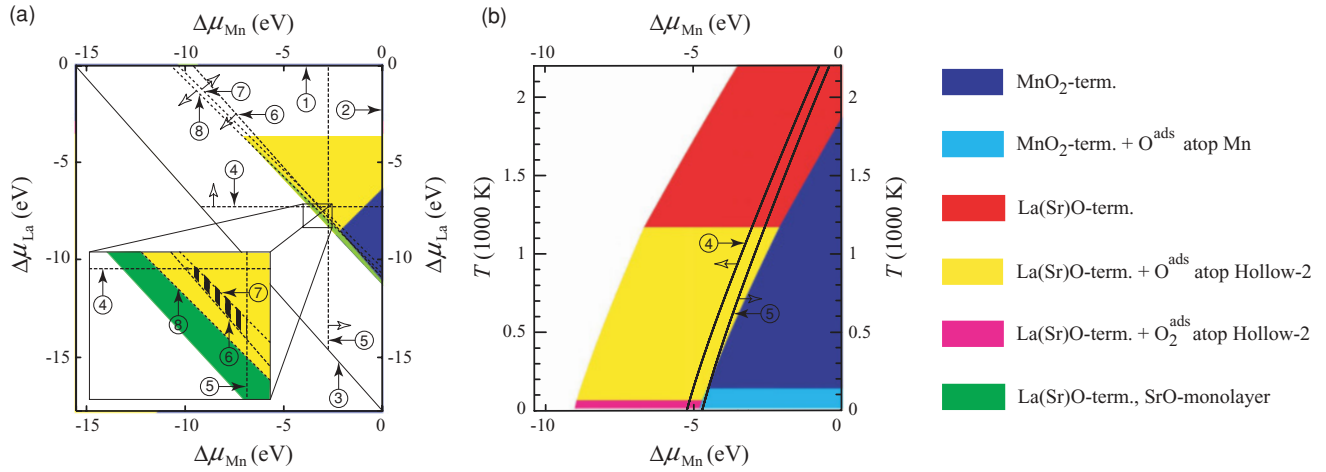


FIG. 2. (Color online) (a) Calculated thermodynamic stability diagram¹¹ for pristine LSM(001) and surfaces covered by oxygen adsorbate (with surface coverage 12.5%, see Fig. 1) at an O_2 partial pressure $p = 0.2p_0$ ($p_0 =$ atmospheric pressure) and $T = 1100$ K (a typical SOFC operational temperature). The region, where LSM ($x = 0.125$) is stable, is the black/yellow (black/gray) cross-hatched area between the $LaMnO_3$, La_2O_3 , Mn_2O_3 , and SrO precipitation lines. Numbers in circles indicate the segregation lines for La (1), Mn (2), Sr (3), La_2O_3 (4), Mn_2O_3 (5), SrO (6), $LaMnO_3$ (7), and $SrMnO_3$ (8). Hollow arrows indicate the regions where precipitation will occur. The inset magnifies the region of LSM stability. (b) The thermodynamic stability diagram calculated along the SrO precipitation line with $\Delta\mu_{La}$ defined according to Eq. (3). The dependence on the oxygen chemical potential is converted to the appropriate temperature scale at an oxygen partial pressure $p = 0.2p_0$. The LSM stability region is bounded by the La_2O_3 (4) and Mn_2O_3 (5) precipitation lines.

to the surface oxygen diffusion process. Taking into account that the most likely oxygen diffusion (transport) path in the LSM cathode is via oxygen ion vacancies we estimated its energetic cost. To create an oxygen vacancy with further O_2 adsorption at an SOFC-relevant temperature of 1100 K 1.6 eV is needed for Mn-LSM(001) and 3.03 eV is needed for La-LSM(001), respectively.

In summary, the non-stoichiometric LSM facilitates significant oxygen transfer between the gas phase and the solid phase.

In this transfer LSM surfaces play an important role. We predict that LSM(001) surfaces at SOFC operating temperature will be covered by chemisorbed O^{-I} species for the Mn-LSM(001) and by O^{-II} species on the La-LSM(001), respectively. Dissociative O_2 adsorption is predicted on La-LSM(001) where chemisorbed O_2 is readily reduced to O_2^{-I} or O_2^{-II} . Our calculations are evidenced by recent thermo-programmed desorption and Fourier transformed infrared spectrometry experiments²² where O_2^{-I} and O_2^{-II} chemisorbed oxygen

TABLE I. Atomic and molecular oxygen adsorption on LSM(001) (see Fig. 1 for labeling of adsorption sites). $l^{M^{surf}-O^{ads}/O_2^{ads}}$ and $P^{M^{surf}-O^{ads}/O_2^{ads}}$ are equilibrium bond length and bond population, respectively, for the bond between the adsorbate O^{ads} or O_2^{ads} and the closest surface atom M^{surf} . $Q^{M^{surf}}$ and $Q^{O^{ads}/O_2^{ads}}$ are the calculated Mulliken effective charges of the surface atoms bonded to the adsorbate and of the adsorbate, respectively. $l^{O_2^{ads}}$ and $P^{O_2^{ads}}$ denote the equilibrium bond length and the O–O bond population of the adsorbed oxygen molecule, respectively. ΔE^{ads} [Eq. (2)] and $\Delta G^{ads}(1100\text{ K}, 0.2p_0)$ [Eq. (1)] are adsorption energy and Gibbs free energy of adsorption under SOFC working conditions, respectively, as calculated with B3LYP hybrid DFT.

Ads. site	M^{surf}	$l^{M^{surf}-O^{ads}/O_2^{ads}}$ (Å)	$P^{M^{surf}-O^{ads}/O_2^{ads}}$ (e)	$Q^{M^{surf}}$ (e)	$Q^{O^{ads}}$ (e)	$l^{O_2^{ads}}$ (Å)	$P^{O_2^{ads}}$ (e)	ΔE^{ads} (eV)	$\Delta G^{ads}(1100\text{ K}, 0.2p_0)$ (eV)
Mn-LSM(001)									
O^{ads}/Mn	Mn	1.58	0.30	1.92 (1.86)	-0.56			-1.32	0.39
O_2^{ads}/Mn	Mn	2.69	0.03	1.86 (1.86)	-0.01	1.24	-0.010	-1.94	1.48
$O^{ads}/O-1$	O	1.45	-0.12	-0.73 (-1.03)	-0.46			-0.03	1.68
$O^{ads}/O-2$	O	1.36	-0.01	-0.45 (-1.20)	-0.26			-0.87	0.84
$O^{ads}/Hollow-1$	Mn	2.33	0.13	1.88 (1.75)	-0.52			1.56	3.27
$O^{ads}/Hollow-2$	O	2.35	0.01	-1.14 (-1.23)	-0.21			1.65	3.36
La-LSM(001)									
O^{ads}/Sr	Sr	2.35	-0.08	1.84 (1.84)	-0.92			-0.40	1.31
O^{ads}/La	La	2.30	0.03	2.35 (2.37)	-0.80			-0.54	1.17
O^{ads}/O	O	1.52	-0.28	-0.89 (-1.63)	-0.83			-1.03	0.68
$O^{ads}/Hollow-1$	La	2.47	0.01	2.37 (2.33)	-0.89			-2.20	-0.49
$O^{ads}/Hollow-2$	La	2.23	0.05	2.28 (2.33)	-1.35			-2.51	-0.80
$O_2^{ads}/Hollow-2$	La	2.50	0.04	2.29 (2.33)	-0.90	1.36	-0.266	-3.20	0.22

species have been identified on the LSM surface in the temperature range between 873 and 1073 K. Another indirect experimental confirmation for our prediction can be derived from the cathodic polarization measurements performed on an LSM cathode pretreated by a dilute HCl solution.²³ Acid etching of the LSM electrode primarily dissolves the surface layer; the experiments showed that mainly Sr and Mn species were etched out from the LSM electrode coating. According to Ref. 23 this treatment leads to a significant improvement of the initial LSM electrode performance, presumably because of improved oxygen surface diffusion. This may possibly indicate that SrO and Mn_xO_y complexes removed from the surface leave behind a bare La-LSM(001), which should be attractive for dissociative oxygen adsorption according to our

calculations, which then would initiate the overall surface oxygen diffusion process. The diffusion of oxygen ions and oxygen vacancies near the LSM surface is supposed to be a rate limiting step for the ORR on LSM cathodes in SOFCs. We will discuss calculated transition states for both Mn- and La-LSM(001) in a forthcoming paper.

This work was partly supported by the Alexander von Humboldt Foundation. S.P. is thankful for the financial support through the ESF project No. 2009/0216/1DP/1.1.1.2.0/09/APIA/VIAA/044. The authors are greatly indebted to E. Kotomin, E. Heifets, R. Merkle, Yu. Matrikov, and J. Maier from the MPI Stuttgart for many fruitful discussions.

*piskunov@lu.lv

¹S. B. Adler, *Chem. Rev.* **104**, 4791 (2004).

²Y. Choi, D. Mebane, J.-H. Wang, and M. Liu, *Top. Catal.* **46**, 386 (2007).

³J. R. Wilson, J. S. Cronin, A. T. Duong, S. Rukes, H.-Y. Chen, K. Thornton, D. R. Mumm, and S. Barnett, *J. Power Sources* **195**, 1829 (2010).

⁴G. J. la O' and Y. Shao-Horn, *Electrochem. Solid-State Lett.* **12**, B82 (2009).

⁵E. A. Kotomin, Y. A. Matrikov, E. Heifets, and J. Maier, *Phys. Chem. Chem. Phys.* **10**, 4644 (2008).

⁶Y. A. Matrikov, R. Merkle, E. Heifets, E. A. Kotomin, and J. Maier, *J. Phys. Chem. C* **114**, 3017 (2010).

⁷Y. Choi, M. C. Lin, and M. Liu, *Angew. Chem. Int. Ed.* **46**, 7214 (2007).

⁸Y. Choi, D. Mebane, M. Lin, and M. Liu, *Chem. Mater.* **19**, 1690 (2007).

⁹Y. Choi, M. E. Lynch, M. C. Lin, and M. Liu, *J. Phys. Chem. C* **113**, 7290 (2009).

¹⁰Y. Choi, M. Lin, and M. Liu, *J. Power Sources* **195**, 1441 (2010).

¹¹S. Piskunov, E. Heifets, T. Jacob, E. A. Kotomin, D. E. Ellis, and E. Spohr, *Phys. Rev. B* **78**, 121406 (2008).

¹²R. A. Evarestov, E. A. Kotomin, Y. A. Matrikov, D. Gryaznov, E. Heifets, and J. Maier, *Phys. Rev. B* **72**, 214411 (2005).

¹³S. Piskunov, E. Spohr, T. Jacob, E. A. Kotomin, and D. E. Ellis, *Phys. Rev. B* **76**, 012410 (2007).

¹⁴A. D. Becke, *J. Chem. Phys.* **98**, 1372 (1993).

¹⁵R. Dovesi, V. R. Saunders, C. Roetti, R. Orlando, C. M. Zicovich-Wilson, F. Pascale, B. Civalleri, K. Doll, N. M. Harrison, I. J. Bush, Ph. D'Arco, and M. Llunell, *CRYSTAL06 User's Manual*, University of Torino, Torino (2006), [<http://www.crystal.unito.it/>].

¹⁶H. J. Monkhorst and J. D. Pack, *Phys. Rev. B* **13**, 5188 (1976).

¹⁷P. Kaghazchi, T. Jacob, I. Ermanoski, W. Chen, and T. E. Madey, *ACS Nano* **2**, 1280 (2008).

¹⁸C. Kan and E. Wachsman, *Solid State Ionics* **181**, 338 (2010).

¹⁹M. W. Chase, *NIST-JANAF thermochemical tables* (American Chemical Society, Washington, DC, 1998).

²⁰K. Reuter and M. Scheffler, *Phys. Rev. B* **65**, 035406 (2001).

²¹Y.-L. Lee, J. Kleis, J. Rossmeisl, and D. Morgan, *Phys. Rev. B* **80**, 224101 (2009).

²²N. Caillol, M. Pijolat, and E. Siebert, *Appl. Surf. Sci.* **253**, 4641 (2007).

²³S. P. Jiang and J. G. Love, *Solid State Ionics* **138**, 183 (2001).